Temperature and Kinematics of CIV Absorption Systems

M. Rauch[1,2], W.L.W. Sargent[1], D.S. Womble[1,2], T.A. Barlow[1]

Subject Headings: Galaxies: formation, evolution — intergalactic medium — quasars: absorption lines

submitted to the ApJ Letters, March 16, 1996 (in press).

Received _____; accepted _____

[1]Astronomy Dept., 105-24 California Institute of Technology, Pasadena 91125

[2]Hubble Fellow

[2]The observations were made at the W.M. Keck Observatory which is operated as a scientific partnership between the California Institute of Technology and the University of California; it was made possible by the generous support of the W.M. Keck Foundation.

ABSTRACT

We use Keck HIRES spectra of three intermediate redshift QSOs to study the physical state and kinematics of the individual components of CIV selected heavy element absorption systems. Fewer than 8% of all CIV lines with column densities greater than $10^{12.5}$ cm^{-2} have Doppler parameters b$<$ 6 kms^{-1}. A formal decomposition into thermal and non-thermal motion using the simultaneous presence of SiIV gives a mean *thermal* Doppler parameter $b_{therm}(CIV)$=7.2 kms^{-1}, corresponding to a temperature of 3.8×10^4K although temperatures possibly in excess of 3×10^5K occur occasionally. We also find tentative evidence for a mild increase of temperature with HI column density. Non-thermal motions within components are typically small (<10 kms^{-1}) for most systems, indicative of a quiescent environment. The two-point correlation function (TPCF) of CIV systems on scales up to 500 kms^{-1} suggests that there is more than one source of velocity dispersion. The shape of the TPCF can be understood if the CIV systems are caused by ensembles of objects with the kinematics of dwarf galaxies on a small scale, while following the Hubble flow on a larger scale. Individual high redshift CIV components may be the building blocks of future normal galaxies in a hierarchical structure formation scenario.

1. Introduction

The CIV $\lambda\lambda$1548,1550 $\AA$ doublet is the most common heavy element absorption feature found in the spectra of high redshift quasars. Most CIV absorption systems must arise in highly ionized (e.g. Bergeron & Stasinska 1986) and strongly clustered gas clouds (e.g. Sargent, Boksenberg & Steidel 1988). Recent Keck observations (Cowie et al. 1995, Tytler et al. 1995) have found CIV absorption to be common for Lyman α forest clouds down to N(HI) $\sim 10^{14}$cm^{-2}. Thus CIV systems trace the gas over the same column density range as the gaseous structures apparently dominating the baryonic contents of the universe (at $z > 2$) (Rauch & Haehnelt 1995, Miralda-Escudé et al. 1996). These systems then may tells us about the physical conditions in the main reservoir of matter, prior to incorporation into virialized galaxies. The precise dynamical state of the individual CIV components has remained elusive. York et al. (1984) established upper limits on the temperature of the gas, ruling out collisional ionization as the dominant equilibrium process. Cowie et al. (1995) found CIV and corresponding HI Lyman α lines to be consistent with clusters of components of photo-heated gas and a small internal velocity dispersion of 18 km/s. To date the existing measurements of the temperature have strictly speaking been upper limits. In the present paper we revisit the thermal and kinematic properties of CIV systems, using high resolution spectroscopy on two ions with different mass to disentangle the contributions of temperature and bulk motion to the line profiles. In particular we ask whether there is a lower limit to the temperature and whether a possible range of temperatures indicates heating sources other than photoionization. We also consider the large scale motion of entire CIV complexes and try to model the velocity structure with a minimum number of

assumptions.

2. The Data

We have observed the spectra of three QSOs, 1225+315, 1107+487, and 1422+231 with the high resolution spectrograph of the Keck telescope. The exposure times were 10500, 26000, and 25100 seconds, respectively, resulting in typical signal-to-noise ratios of 20-35 (1225+315), 30-45 (1107+487), and 55-85 (1422+231) per 0.04 $\AA$ pixel. The observation of Q1225+315 was done with a 0.57 arcsec wide slit to achieve very high resolution of 5.3 kms^{-1} (FWHM; as measured from a ThAr spectrum) for the final linearized and summed data, with the explicit purpose of trying to resolve the thermal width of the CIV doublet. The spectra of the other two objects were obtained with a 0.86 arcsec slit (FWHM 6.6 km^{-1}). The data were reduced as described in Barlow & Sargent (1996, in prep.). A continuum was fitted with spline functions, and the line profiles where fitted with the Voigt profile package VPFIT (e.g. Carswell et al. 1991) The complete data sets will be published elsewhere together with the analysis of the Lyα forest regions.

3. Analysis of the absorption line profiles

Figure 1 (top) shows the Doppler parameter - column density distribution (b - log N(CIV)) for all CIV components in the spectrum of Q1225+317 (the highest resolution data set) longward of Lyα emission and with column densities above logN(CIV)=12. The dotted line indicates the lowest Doppler parameter resolvable in any region of the spectrum, 3.18 kms^{-1} (5.3 kms^{-1} FWHM). Wherever possible

these parameters were obtained from fits to both lines of the CIV doublet. Note that the large majority of CIV lines are resolved. Given the size of the error bars, quite a number of points should have scattered below the dotted line if there were many lines close to or narrower than the resolution limit. The bottom panel shows the same distribution for the full sample of all 3 QSOs. Fig. 2 gives a Doppler parameter histogram for the full sample. Mean and median Doppler parameters are 9.3± 0.7 kms^{-1}, and 10.6 kms^{-1}, respectively. Only 15 % of the lines have b values below 6 kms^{-1}; for those lines with logN >12.5 the fraction is lower at 8 %. 81% of all lines have b < 16 kms^{-1}.

To separate the contributions of thermal and non-thermal motion ("bulk motion", or "turbulence") we use the simultaneous presence of the CIV and SiIV ion, and we assume that the bulk motion can be represented by a Gaussian (our main conclusions regarding the temperature range are not strongly dependent on the exact method of deconvolution). Then we can write

$$b_i^2 = b_b^2 + \frac{2kT}{m_i}, (i = 1, 2), \tag{1}$$

where the index i denotes the ion used, in our case CIV (1) and SiIV (2). We solve these equations for T and b_b. This procedure is based on the assumption that CIV and SiIV have the same temperature and bulk motion in each cloud, inspite of their rather different ionization potentials. This assumption need not be universally true, but it holds for a pressure confined static gas cloud; hydrodynamic simulations (Haehnelt, Steinmetz & Rauch 1996) indicate that it is also approximately valid for gravitationally collapsed clouds, because the spatial extent of the regions dominating the line formation is determined by the spatial scale of highest peaks in the total gas density, even for higher ions, and the ionization fraction is only of secondary

importance.

We solved the equations (1) for a sample of 79 of the 208 CIV absorption systems for which both CIV and SiIV were available. We have fitted the absorption complexes requiring the SiIV components to have the same redshifts as CIV. We have retained in our analysis only the CIV and SiIV absorption line pairs with fractional errors of less than 20 % in their Doppler parameters in order to eliminate ill-constrained cases caused by run-away profile fits, noisy weak lines, and severe blending. Five cases where the best fit Doppler parameter of SiIV, b(SiIV), ended up larger than b(CIV) were excluded from the analysis as being unphysical. For the surviving sample of 26 CIV/SiIV pairs we computed the thermal Doppler parameter of the CIV component from

$$b^2_{therm_{CIV}} = \frac{b^2_{CIV} - b^2_{SiIV}}{1 - \frac{m_C}{m_{Si}}}. \quad (2)$$

The sample $b_{therm}(CIV)$ versus total Doppler parameter $b(CIV)$ is plotted in figure 3. The solid lines are the loci of constant bulk motion, beginning with zero, i.e., pure thermal motion ($b_{therm}(CIV) = b(CIV)$) on the upper left and proceeding to $b_b(CIV) = 20$ kms^{-1} in steps of 5 kms^{-1}. The dashed line denotes equipartition between thermal and non-thermal energy. The measured thermal Doppler parameters tend to lie mostly between the zero and the 10 kms^{-1} bulk motion line. The mean of the *thermal* CIV b parameter for this sample is $\overline{b_{therm}(CIV)} = 7.2$ kms^{-1}, The corresponding value for the *total* CIV Doppler parameter is $\overline{b(CIV)} = 9.6$ kms^{-1}, similar to that of the full sample of CIV lines. The medians are $b^{med}_{therm}(CIV) = 9.9$ kms^{-1}, and for the total width $b^{med}(CIV) = 12.6$ kms^{-1}, somewhat higher than the means because of a tail in the distribution towards large Doppler parameters with relatively larger errors. A "typical" value for the bulk motion contribution is then

given by

$$b_b(CIV) = \sqrt{\overline{b(CIV)}^2 - \overline{b_{therm}(CIV)}^2} = 6.3\ kms^{-1} \quad (3)$$

It appears that this value is not representative of the full range in b as it is dominated by the low b lines which have smaller errors. An apparent increase of $b_b(CIV)$ with the total b(CIV) beyond 15 kms^{-1} formally implies that hotter gas also has more bulk motion. However, some of the broader lines may well be blends, so in theses cases we may be overestimating the non-thermal component. In any case, it is clear that the kinetic energy of the gas causing these high ionization absorption systems is dominated by thermal energy, and that the contribution from turbulence or other (quasi-Gaussian) bulk motions are small. Even if we remain sceptical about the Gaussian assumption we can always take the total Doppler parameters as *upper limits* to any contribution from bulk motion.

The value $\overline{b_{therm}(CIV)} = 7.2$ kms^{-1} translates into a temperature T $\approx$ 38000 K, or a thermal contribution to the Lyα line width $b_{therm}(HI)$ of 25.0 kms^{-1}. If, as we have seen, above the thermal Doppler parameter occupies a relatively narrow range some of the broadest HI Lyα lines must be due to unresolved clusters (Rauch et al. 1992). Therefore, the difference between the average total Doppler parameter for the Lyman α forest and the smaller thermal widths measured here may indeed often be one of small scale velocity dispersion among several individual CIV components, as suggested by Cowie et al. (1995).

If we take the minimum HI Doppler parameter ($\sim$ 20 kms^{-1}) of the *lower* column density ($3 \times 10^{13} < N(HI) < 3 \times 10^{14}$) systems in the Hu et al. (1995) Lyα forest sample to correspond to pure thermal broadening then the thermal HI b parameter extrapolated from our *higher* column density (all lines correspond to

$N(HI) >$ a few times 10^{14}) CIV sample indicates a mild increase of b with N(HI), with b_{therm}(HI) rising from $\sim$ 20 to 25 kms^{-1} (T from 2.5-3.8$\times 10^4$ K), while the column density increases by at least a factor 10. Taken together with our finding of a range of temperatures up to 3×10^5 K and possibly beyond (fig. 3), this implies that not all high column density, broader absorption lines are small clusters of subunits with a uniform, low temperature.

4. Understanding the kinematics of CIV systems

The two point auto-correlation function (TPCF) of the full CIV sample is given in figure 4, out to a pair splitting of 700 kms^{-1}. The amplitude of each bin of the TPCF has been normalized by the expected number of counts per bin for a random distribution of clouds.

After a steep decline within the first 200 kms^{-1} there is a flattening in the TPCF out to about 400 kms^{-1}, before the amplitude drops to the average value or even below. Following Petitjean and Bergeron (1990,1994, hereafter PB) we can model the shape of the TPCF formally by fitting 3 Gaussians to the data, with velocity dispersions σ=22, 136 and 300 kms^{-1}, respectively. PB found a best fit for two Gaussians, with σ values of 80 and 390 kms^{-1} for a $< z >\sim$ 1 MgII sample, and σ's of 109 and 525 kms^{-1} for a CIV sample with $< z >$=2.65. In our CIV data the third Gaussian was required to match the narrow peak at zero velocity; such a detail may not have been obvious in the PB sample. The similarity between the MgII and CIV TPCFs is quite striking, as PB noted, and this coincidence may be an argument in favour of QSO absorbers being small clouds each with high and low ionization zones subject to the same kinematical conditions, rather than large onion

shell structures.

The large velocity splittings in the observed TPCF may result from ordered large scale motion rather than isotropic random velocity dispersion. Accordingly, we investigate a simple model, where a set of identical "absorbers" occupies random positions within an extended sheet, which in reality may represent galaxies embedded in a large scale wall of gas. The sheet is taken to expand with the Hubble flow, and the individual absorption components are assumed to have an internal isotropic Gaussian velocity distribution. We have computed the TPCF by running randomly directed lines-of-sight through the centers of these slabs. The result of one such calculation are shown overplotted as a dotted line on the observed TPCF in figure 4. For this realization, the sheets were 1.5 Mpc long and wide, and 60 kpc thick, and the Hubble constant was 550 kms^{-1} Mpc^{-1} (at z=2.78). The internal velocity dispersion among the components was σ =20 kms^{-1}, and the absorbers had hard boundaries with radii of 45 kpc. The number density of absorbers *within the sheets* was 300 Mpc^{-3}, with the overall normalization chosen such as to match the observed TPCF. Obviously, a simple model with a small internal velocity dispersion coupled with an nonisotropic expansion of randomly oriented sheets of clouds can match the measured TPCF quite well. This probably does not rule out alternative models where the velocity splitting is dynamical, e.g. with CIV systems orbiting in large galactic halos ($v_c \sim 200$ kms^{-1}), but it seems that deep potential wells are *not required* to explain the TPCF. If this picture of smallish CIV clumps in expanding, coherent large scale walls (surrounding voids) is correct, the *largest velocity splitting* is then a measure of the product of Hubble constant and coherence length of the walls, $\Delta v_{max} \approx H(z)L(z)$. This quantity increases with redshift only $\propto (1+z)^{\frac{1}{2}}$ (q_0=0.5), so we should expect the temporal evolution of the high velocity tail of the

TPCF to be weak, consistent with PB's observed small difference between the low z MgII and high z CIV correlation functions.

5. Conclusions

The kinetic energy of each individual CIV component is dominated by thermal motions with average temperature $\sim$ 38000 K, occasionally ranging up to a few hundred thousand degrees. The lower limit to the CIV Doppler parameter and a likely positive correlation between temperature and column density also point to gas heated by photoionization, perhaps compressed under the influence of a shallow potential well. However, individual CIV components do not display a velocity broadening characteristic of the full virial velocity of a massive galaxy but are at best compatible with the velocity dispersion in dwarf spheroidals (e.g. Hargreaves et al. 1994). To produce line widths as small as measured, the individual clouds must be rather quiescent and could be confined quasi-statically by an isotropic outer pressure from a hotter medium (e.g. Mo 1994). Alternatively, since the absorption line optical depth is proportional to the gas density, the CIV lines could arise in spatially small, collapsed regions (e.g., cooling gas at rest behind an accretion shock), where the strong density gradients assure that only the quiescent, narrow density peaks contribute noticeably to the line profile.

A simple model of an ensemble of absorbing objects with small internal velocity dispersion, embedded in flattened large scale "walls" expanding with the Hubble flow can explain the measured TPCF, including the narrow maximum at the smallest splittings, and the tail out to 400km/s, which in this model is due to chance alignments of our line of sight with the expanding large scale structure.

The large velocity spreads of many hundred km/s and the quiescent structure of the individual components are consistent with the identification of CIV systems with groups of protogalactic clumps ($M_{baryon} \sim 10^9 M\odot$) in a hierarchical structure formation scenario (Haehnelt, Steinmetz & Rauch 1996, Rauch et al. in prep.). If this conjecture should turn out to be correct, high resolution observations of CIV systems should be able to provide us with unprecedented insights into gravitational galaxy formation at high redshift.

DSW and MR are grateful to NASA for support through grants HF-1040.01-92A and HF-01075.01-94A from the Space Telescope Science Institute. WLWS was supported by grant AST92-21365 from the National Science Foundation. We thank Martin Haehnelt for discussions, Bob Carswell and John Webb for providing us with their profile fitting software, and the W.M. Keck Observatory Staff for their help with the observations.

REFERENCES

Bergeron, J, Stasinska, G., 1986 A&A, 169,1

Carswell, R.F., Lanzetta, K.M., Parnell, H.C., Webb, J.K., 1991, ApJ, 371, 36

Cowie, L.L., Songaila, A., Kim, T.-S., and Hu, E.M., 1995 AJ, 109, 1522

Haehnelt, M.G., Steinmetz, M., Rauch, M., 1996,ApJ, in press.

Hargreaves, J.C., Gilmore, G., Irwin, M.J., and Carter, D., 1994, MNRAS, 269, 957

Hu, E.M., Kim, T.-S., Cowie L.L., Songaila, A., Rauch, AJ, 110, 1526

Miralda-Escudé, J., Cen, R., Ostriker, J., Rauch, M., 1996, ApJ, (in press)

Mo, H.J., 1994, MNRAS, 269, L49

Petitjean, P., Bergeron, J., 1990, A&A, 231, 309

Petitjean, P., Bergeron, J., 1994, A&A, 283, 759

Rauch, M., Carswell, R.F., Chaffee, F.C., Foltz, C.B., Webb, J.K., Weymann, R.J., Bechtold, J., Green, R.F., 1992, ApJ, 390, 387

Rauch, M., Haehnelt, M.G., 1995, MNRAS, 275, L76

Sargent, W.L.W., Boksenberg, A., Steidel, C.C., 1988, ApJ, 68, 539

Tytler D., Fan X.-M., Burles S., Cottrell L., Davis C., Kirkman D., Zuo L., 1995, in *QSO Absorption Lines*, Proc. ESO Workshop, ed. G.Meylan (Heidelberg: Springer), p. 289.

York, D.G., Green, R.F., Bechtold, J., Chaffee, F.C., 1984, ApJ, 280, L1

This manuscript was prepared with the AAS LaTeX macros v4.0.

Figure captions:

Fig. 1.— Above: Doppler parameter versus column density for CIV systems in the line-of-sight to QSO 1225+315. Below: the same plot for the full sample of 208 CIV components. The dotted line gives the minimum resolution attained in each sample. Two points (probable run-away fits) at 41 and 57 km/s are off the edges.

Fig. 2.— Doppler parameter histogram for the full sample

Fig. 3.— thermal versus total CIV Doppler parameter for 26 systems selected to have small relative errors in both b(CIV) and b(SiIV). The solid curves are lines of constant non-thermal motion, the dashed line is the locus of equipartition between thermal and non-thermal energy.

Fig. 4.— two-point correlation function (TPCF) for the full CIV sample, normalized by the expected number of pairs per bin for a random distribution in redshift space. The dotted line is the TPCF for the expanding-sheet model described in the text.

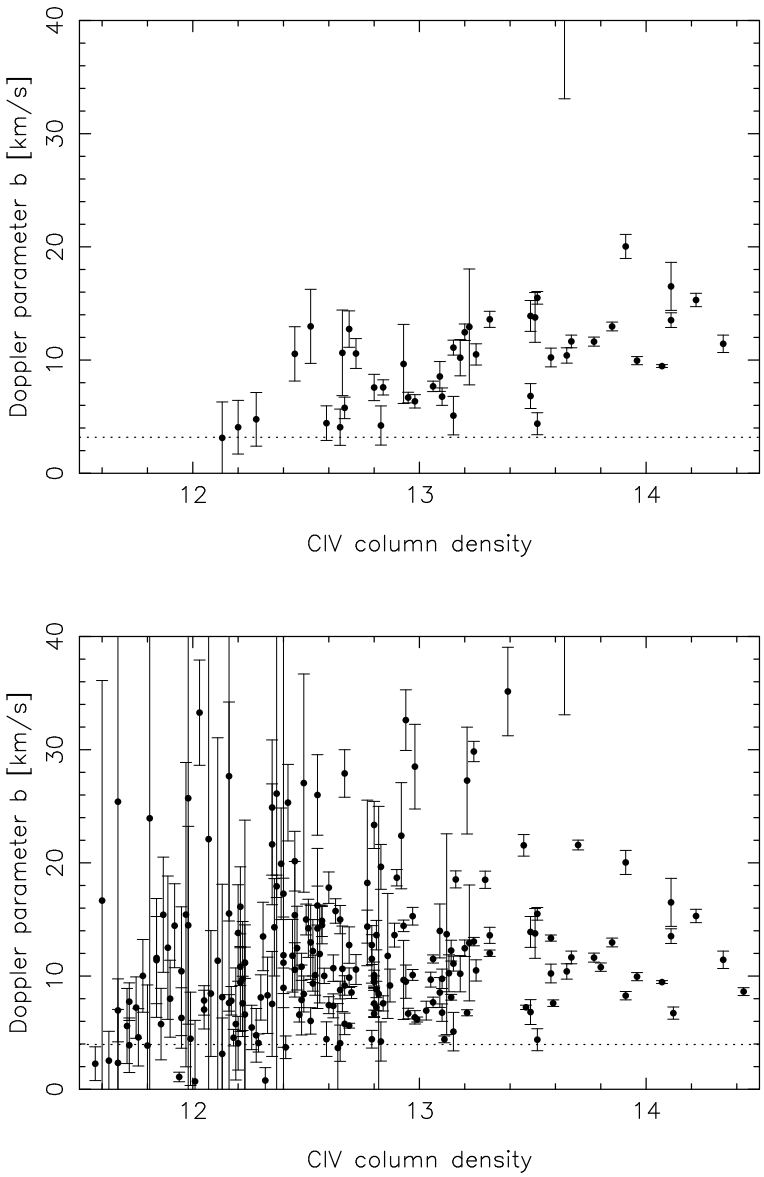
Doppler parameter b [km/s]
0
10
20
30
40
12
13
14
CIV column density
Doppler parameter b [km/s]
0
10
20
30
40
12
13
14
CIV column density

Figure 1

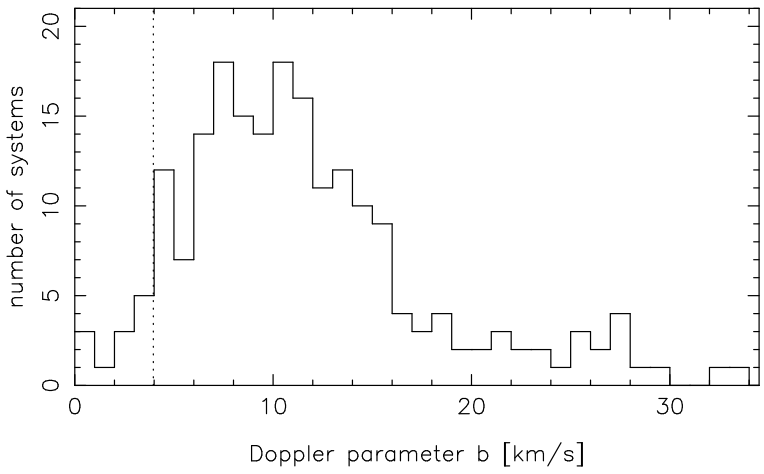
number of systems
0
5
10
15
20
0
10
20
30
Doppler parameter b [km/s]

Figure 2

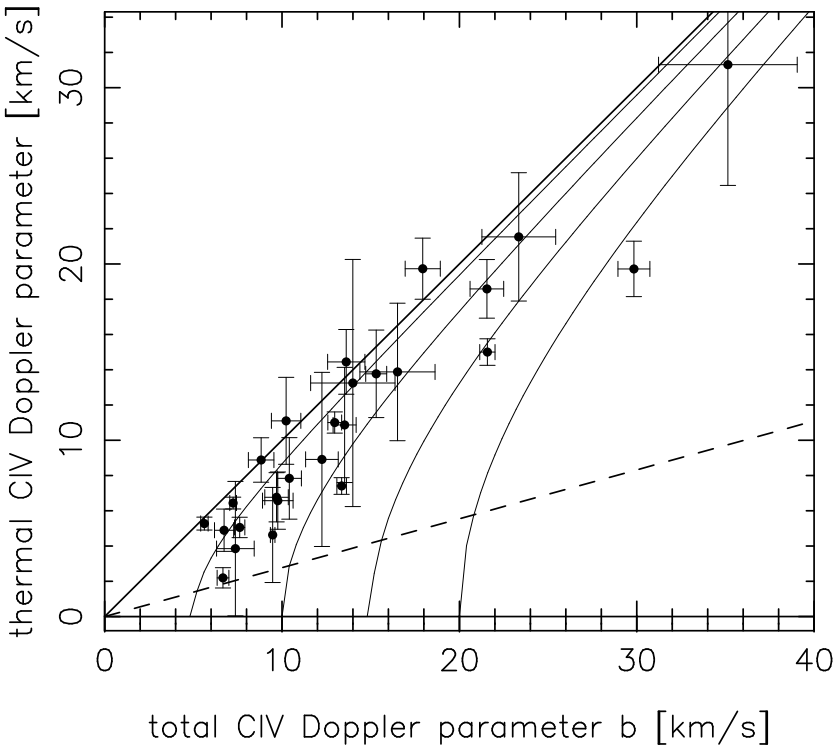
thermal CIV Doppler parameter [km/s]
total CIV Doppler parameter b [km/s]
0
10
20
30
40

Figure 3

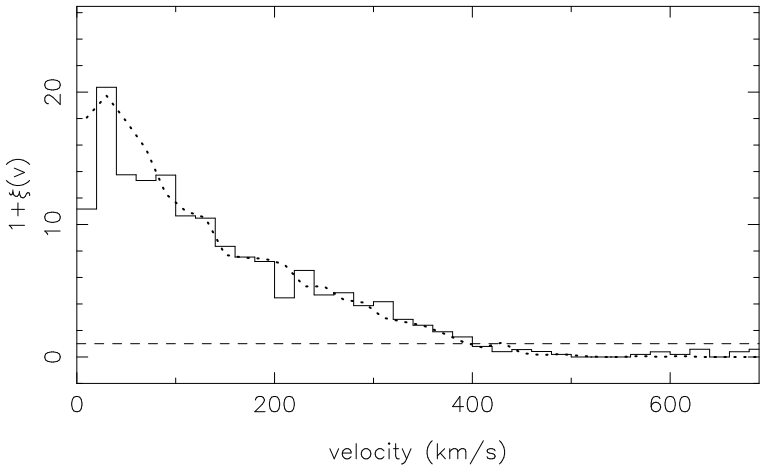

Figure 4